Year: 2012

Src42A-dependent polarized cell shape changes mediate epithelial tube elongation in Drosophila

Dominique Förster, Stefan Luschnig

Originally published at:
Förster, Dominique; Luschnig, Stefan (2012). Src42A-dependent polarized cell shape changes mediate epithelial tube elongation in Drosophila. Nature Cell Biology, 14(5):526-534, http://dx.doi.org/10.1038/ncb2456.

nature cell biology

Src42A-dependent polarized cell shape changes mediate epithelial tube elongation in *Drosophila*

Dominique Förster[1] and Stefan Luschnig[1,2]

Although many organ functions rely on epithelial tubes with correct dimensions, mechanisms underlying tube size control are poorly understood. We analyse the cellular mechanism of tracheal tube elongation in *Drosophila*, and describe an essential role of the conserved tyrosine kinase Src42A in this process. We show that *Src42A* is required for polarized cell shape changes and cell rearrangements that mediate tube elongation. In contrast, diametric expansion is controlled by apical secretion independently of *Src42A*. Constitutive activation of *Src42A* induces axial cell stretching and tracheal overelongation, indicating that *Src42A* acts instructively in this process. We propose that *Src42A*-dependent recycling of E-Cadherin at adherens junctions is limiting for cell shape changes and rearrangements in the axial dimension of the tube. Thus, we define distinct cellular processes that independently control axial and diametric expansion of a cylindrical epithelium in a developing organ. Whereas exocytosis-dependent membrane growth drives circumferential tube expansion, *Src42A* is required to orient membrane growth in the axial dimension of the tube.

Epithelial cells generate tubules of precisely defined dimensions and shapes. Although widespread diseases, such as polycystic kidney disease, are due to aberrant tube size, mechanisms that control tubule dimensions are only partially understood[1,2]. Tracheal tubes in *Drosophila* expand in length and diameter to generate airways of stereotyped dimensions[3]. Distinct kinetics of axial and diametric tracheal tube expansion suggested that the two processes are controlled separately[4]. Exocytosis-dependent apical (luminal) membrane growth drives diametric expansion[5,6], whereas a luminal extracellular matrix is essential to prevent excessive tube expansion[7–10]. However, the mechanism that mediates tube elongation remained unknown.

In wild-type embryos the tracheal dorsal trunk elongates approximately twofold over three hours[4] (Supplementary Movie S1). We identified two mutations in the *Src42A* gene[11,12], which were defective in dorsal-trunk elongation (Fig. 1a–d). The dorsal trunk was 34% shorter and the transverse connectives were 54% shorter than in wild-type embryos (Fig. 1e,f), whereas overall embryo length was unchanged. Furthermore, dorsal-trunk luminal diameter in *Src42A* mutants was 15% larger than in controls, indicating that *Src42A* mutations lead to altered tube proportions, rather than a deficit in tube elongation. Interestingly, whereas the multicellular dorsal-trunk and transverse-connective branches were short, the unicellular dorsal and ganglionic branches were normal in length (Fig. 1f and data not shown), indicating that *Src42A* specifically affects elongation of multicellular tracheal tubes. Tracheal-specific expression of a dominant-negative *Src42A* construct (*Src42A.KM*; ref. 11) led to short dorsal trunks similar to those of *Src42A* mutants (Fig. 1e and Supplementary Fig. S1c). Tube elongation in *Src42A* mutants was restored by tracheal-specific expression of *Src42A*, indicating that *Src42A* function is required in tracheal cells for tube elongation (Fig. 1g). Targeting *Src42A* expression to just three posterior body segments restored tube elongation only in the corresponding tracheal metameres. Adjacent anterior metameres lacking wild-type *Src42A* expression remained short, indicating that *Src42A* acts cell-autonomously (Fig. 1h).

We analysed Src42A protein distribution in tracheal cells. Whereas Src42A protein was distributed along the entire plasma membrane, activated Src42A was largely restricted to adherens junctions, as detected by an antibody against Src42A phosphorylated on Tyr 400 (pSrc; ref. 11; Supplementary Fig. S1). In $Src42A^{F80}$ embryos, Src42A protein levels and membrane localization seemed normal. However, pSrc signals were abolished, indicating that the ATP-binding site mutation in $Src42A^{F80}$ may render the kinase non-activatable without affecting protein stability or membrane localization. These results indicate that Src kinase activity is essential for tracheal tube elongation. Although $Src42A^{F80}$ behaved as a recessive loss-of-function mutation in genetic tests (data not shown), tube elongation defects of $Src42A^{F80}$ embryos were slightly stronger than those of $Src42A^{26-1}$ null mutants. This may be explained by competition of the $Src42A^{F80}$ protein with maternally supplied wild-type Src42A or with the partially redundant Src64B (refs 13,14).

We analysed the cellular basis of the *Src42A* phenotype in living embryos (Fig. 2). Apical surfaces of dorsal-trunk cells in stage-16 *Src42A* mutants were on average 22% smaller than in controls

[1]Institute of Molecular Life Sciences (IMLS) and Ph.D. Program in Molecular Life Sciences, University of Zurich, 8057 Zurich, Switzerland.
[2]Correspondence should be addressed to S.L. (e-mail: stefan.luschnig@imls.uzh.ch)

Received 20 December 2011; accepted 7 February 2012; published online 25 March 2012; DOI: 10.1038/ncb2456

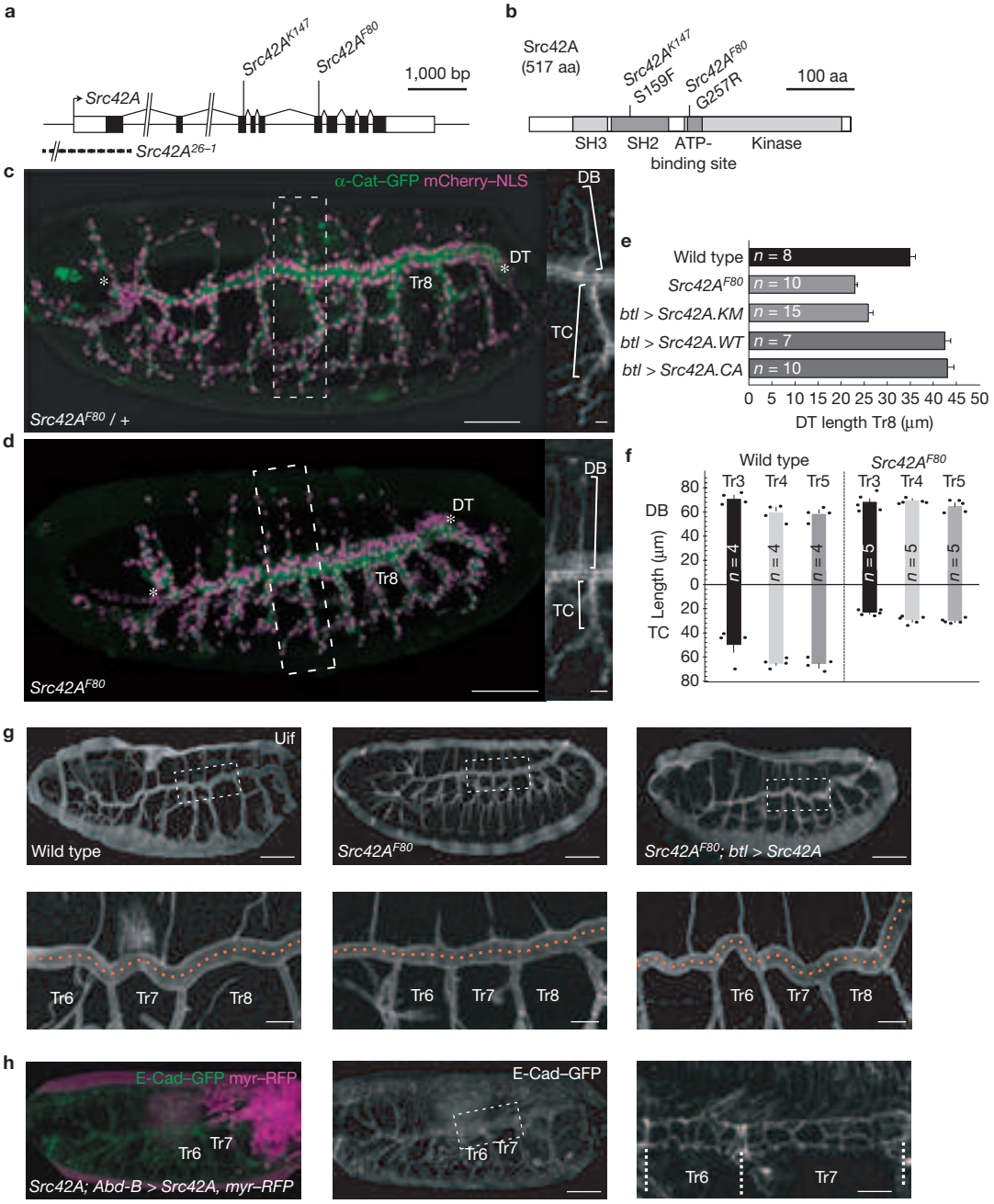

Figure 1 *Src42A* is required for tracheal tube elongation. (**a**,**b**) *Src42A* gene (**a**) and protein (**b**). The *Src42A*^{K147} and *Src42A*^{F80} mutations cause amino-acid (aa) exchanges in the SH2 domain (*Src42A*^{K147}: S159F) and the ATP-binding site (*Src42A*^{F80}: G257R) of the kinase domain, respectively. The deleted region in *Src42A*$^{26-1}$ is indicated by a dashed line. (**c**,**d**) Living stage-15 heterozygous (**c**) and homozygous (**d**) *Src42A*^{F80} embryos expressing α-Cat–GFP (green) and mCherry–NLS (nuclear localization sequence, magenta) in tracheal cells. Ends of the dorsal trunk (DT) are indicated by asterisks. The position of tracheal metamere eight (Tr8) is indicated. Close-ups to the right show dorsal branches (DB) and transverse connectives (TC) in Tr5 (boxed areas). Note that in *Src42A*^{F80} mutants dorsal trunks and transverse connectives remain short, whereas dorsal branches elongate normally. Embryo length in *Src42A* mutants (470 ± 6 μm) is not significantly different from that of wild-type embryos (481 ± 4 μm; $n = 10$, $P = 0.14$). Scale bars, 50 μm; close-ups, 10 μm. (**e**) Quantification of dorsal-trunk length in Tr8 in wild-type embryos, *Src42A*^{F80} mutants, and embryos expressing either wild-type *Src42A.WT*, dominant-negative *Src42A.KM* or constitutively active *Src42A.CA* in tracheal cells. Dorsal-trunk length is significantly reduced in *Src42A*^{F80} mutants ($P = 1.64 \times 10^{-6}$) and in *Src42A.KM*-expressing embryos ($P = 1.54 \times 10^{-6}$), and is significantly increased in embryos expressing either wild-type ($P = 1.0 \times 10^{-3}$) or constitutively active *Src42A* ($P = 4.4 \times 10^{-4}$). Error bars, s.e.m. (**f**) Quantification of dorsal-branch and transverse-connective length in Tr3–5 in wild-type and *Src42A*^{F80} embryos. Error bars, s.e.m. (**g**) Stage-16 embryos stained for Uif. Tracheal-specific expression of wild-type *Src42A* rescues dorsal-trunk and transverse-connective elongation in *Src42A*^{F80} mutants. The dorsal-trunk lumen is indicated by a dashed line. Scale bars: upper panels, 50 μm; lower panels, 10 μm. (**h**) Living stage-16 *Src42A*^{F80} embryo expressing *Src42A* in posterior body segments, including tracheal metameres Tr7–10. *Src42A*-expressing cells are marked by myr–RFP (magenta). Adherens junctions are marked by E-Cad–GFP (green). Dashed lines in close-up (right) indicate tracheal metamere borders. Note that dorsal-trunk elongation is restored only in the *Src42A*-expressing part of the dorsal trunk. The ratio of Tr7/Tr6 metamere lengths was 0.96 ± 0.02 in *Src42A*^{F80} mutants and 1.58 ± 0.11 in *Src42A*^{F80}; *Abd-B-Gal4/UAS-Src42A* embryos ($n = 6$). Scale bar, 50 μm; close-up (right panel), 10 μm.

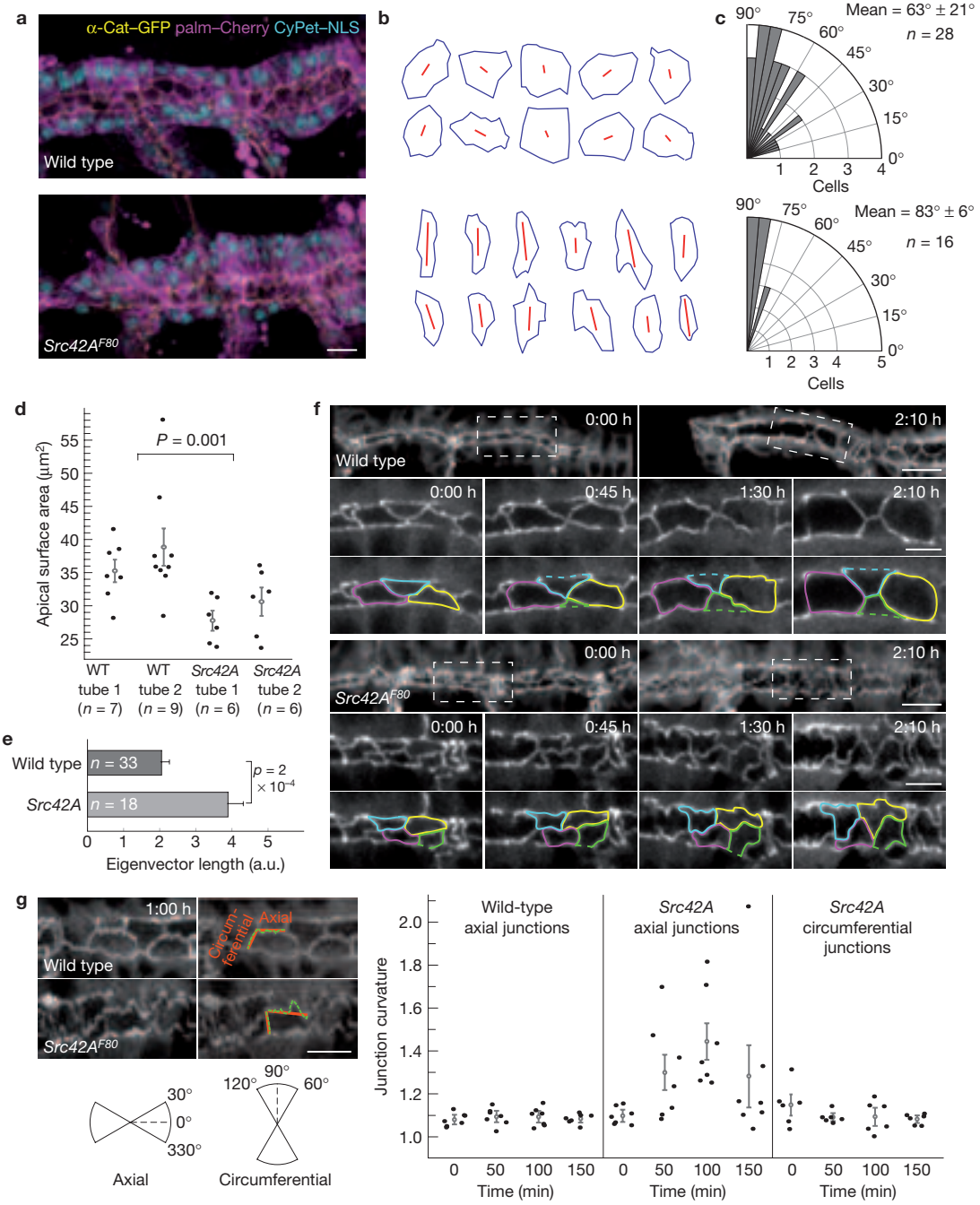

Figure 2 *Src42A*-dependent cell shape changes and cell rearrangements mediate dorsal-trunk elongation. (**a**) Living stage-16 wild-type and *Src42A*^{F80} embryos expressing α-Cat–GFP (yellow), palmitoylated mCherry (magenta), and CyPet–NLS (cyan). Scale bar, 10 μm. (**b**) Two-dimensional projections of dorsal-trunk cell apical outlines in Tr8 in wild-type (top) and *Src42A*^{F80} -mutant (bottom) embryos. Eigenvectors (red lines) indicate the orientations of apical cell surfaces. The tube axis is horizontal. (**c**) Angle distribution of apical surface eigenvectors. The tube axis was set to 0°. Note that angles are broadly distributed in the wild type, but biased towards circumferential orientation in *Src42A*^{F80} mutants ($P = 6.0 \times 10^{-5}$). (**d**) Apical surface areas of wild-type (WT) and *Src42A*^{F80} dorsal-trunk cells. Two wild-type and two mutant embryos with comparable dorsal-trunk cell numbers in Tr8 (26 ± 1 cells) were analysed. Open circles and error bars, mean values ± s.e.m. (**e**) Lengths of apical surface eigenvectors (arbitrary units) of wild-type and *Src42A*^{F80} dorsal-trunk cells. Apical surfaces of *Src42A*^{F80} cells are elongated when compared with those of wild-type cells. Error bars, s.e.m. (**f**) Stills from time-lapse movies of dorsal-trunk expansion in wild-type (upper panels) and *Src42A*^{F80} (lower panels) embryos expressing α-Cat–GFP (Supplementary Movie S2). Close-ups of the areas marked by white rectangles are shown. Apical outlines of selected dorsal-trunk cells are highlighted in colour. Whereas wild-type dorsal-trunk cell surfaces expand both axially and circumferentially and undergo cell rearrangements, apical cell profiles in *Src42A* expand more slowly and only circumferentially. Note the partial cell-intercalation event that separates the yellow-labelled cell and the magenta-labelled cell in the wild-type dorsal trunk (upper panels). Scale bar, 5 μm. (**g**) Curvature of apical cell boundaries was calculated as the ratio of traced junction length (green lines) and vertex distance (red lines) at four times during dorsal-trunk expansion. Note that junctions in the wild type remain relatively straight during dorsal-trunk expansion, whereas in *Src42A* mutants axial (0° ± 30°; $n = 7$), but not circumferential (90° ± 30°; $n = 6$), junctions become corrugated over time. Filled circles, values for single junctions; open circles and error bars, mean values ± s.e.m. (P values for axial junction curvature in wild-type versus *Src42A*^{F80}: $t_0 = 0.37$; $t_{50} = 0.05$; $t_{100} = 0.006$; $t_{150} = 0.19$). Scale bar, 5 μm.

(Fig. 2a,b,d). Furthermore, the shapes and orientations of apical cell surfaces were strikingly altered. Cell surfaces were elongated circumferentially (Fig. 2b,e). Orientations of apical surface eigenvectors were broadly distributed in the wild type, but were biased towards circumferential orientation in *Src42A* mutants (Fig. 2c). These effects on cell shape explain the altered tube proportions (shorter but wider dorsal trunk) in *Src42A* mutants.

To understand the cell behaviours underlying dorsal-trunk elongation, we carried out time-lapse imaging (Fig. 2f,g and Supplementary Movie S2). Whereas apical surfaces of wild-type dorsal-trunk cells expanded both circumferentially and axially, *Src42A* mutant cells expanded only circumferentially. Apical cell junctions remained straight during dorsal-trunk expansion in wild-type embryos, whereas in *Src42A* mutants axially, but not circumferentially, oriented junctions became increasingly corrugated, indicating that *Src42A* is specifically required for axially oriented cell surface expansion, rather than for apical membrane growth *per se* (Fig. 2g). Furthermore, we observed sporadic conversions of circumferential junctions into axial junctions, resembling partial cell-intercalation events, in wild-type, but not *Src42A* mutant, embryos (Fig. 2f). Thus, axially oriented apical membrane expansion and polarized cell rearrangements contribute to dorsal-trunk elongation in a *Src42A*-dependent manner, whereas circumferential cell surface expansion is independent of *Src42A* function.

We asked whether altered dorsal-trunk cell orientation in *Src42A* mutants may be due to a corresponding change in planar cell polarity (PCP) in the tracheal epithelium. The regular circumferential arrangement of taenidial rings[15] was not affected in $Src42A^{F80}$ mutants, indicating that global planar tissue polarization may be unchanged (Fig. 4c below). Consistent with earlier work[16], we found no evidence for polarized distribution of the PCP pathway components Flamingo (Fmi, also known as Stan; ref. 17) and Strabismus (Stbm (also known as Vang)–YFP (yellow fluorescent protein); ref. 18) in wild-type tracheal dorsal trunk (Supplementary Fig. S2). To probe a potential role of *Src42A* in PCP signalling, we therefore analysed the effect of dominant-negative *Src42A.KM* on PCP in the wing[19]. *Src42A.KM* expression in the posterior wing compartment caused severe morphological abnormalities, including reduced wing size and disorganized wing hairs. Despite these defects, the polarized localization of Fmi at proximal and distal cell membranes in pupal wings was unaffected, indicating that PCP signalling was intact. These results suggest that *Src42A* is not involved in PCP signalling.

Src42A mutants also showed abnormal epithelial organization. Whereas wild-type dorsal-trunk cells were cuboidal with nuclei distributed in a single layer, *Src42A*-mutant cells were markedly elongated perpendicular to the tube axis and nuclei seemed to stack on one another, resembling a pseudostratified epithelium (Fig. 2a). This effect was limited to the dorsal side of posterior dorsal-trunk metameres and became apparent during stage 14, concurrent with the onset of dorsal-trunk elongation in wild-type embryos (Supplementary Fig. S3). To analyse epithelial organization in more detail, we adapted the Brainbow system[20] for tracing surfaces of individual tracheal cells (Fig. 3a–f). The longest axis of dorsal-trunk cells was on average 23% longer in *Src42A* mutants when compared with controls (Fig. 3g). Furthermore, *Src42A* cells were oriented perpendicular to the tube axis, whereas orientations of wild-type cells were distributed more broadly (Fig. 3c,e,h). Despite the apparent stacking of nuclei in *Src42A* mutants, most dorsal-trunk cells reached both the luminal and the basal surface, indicating that the epithelium is not multilayered, but pseudostratified (Supplementary Movies S3 and S4). Thus, single-cell analyses indicate that *Src42A* is required for maintaining columnar epithelial organization during dorsal-trunk expansion, suggesting that *Src42A*-dependent epithelial remodelling promotes tracheal tube elongation.

To address whether *Src42A* plays a permissive or instructive role in dorsal-trunk elongation, we overexpressed either wild-type Src42A or a constitutively activated Src42A kinase (*Src42A.CA*; ref. 14) in tracheal cells. Expression of either construct led to overelongated and convoluted dorsal trunks (Figs 4 and 1e). Activated Src42A caused the most severe effects, including partially penetrant lumen fusion defects (not shown). *Src42A.CA*-expressing embryos showed 23% longer dorsal-trunk metameres when compared with controls, although dorsal-trunk cell number was unchanged (Figs 1e, 4a and Supplementary Fig. S1c). *Src42A.CA*-expressing dorsal-trunk cells were flattened and markedly elongated axially, indicating that *Src42A*-induced cell shape changes may account for excessive tube elongation following Src42A activation (Fig. 4b). These results indicate that Src42A kinase activity is necessary and sufficient for elongation of tracheal cells along the tube axis and suggest that *Src42A* plays an instructive role in promoting elongation of multicellular tracheal tubes.

It is possible that this instructive role of Src42A is mediated by planar polarized Src kinase activity, resulting in locally confined regulation of Src substrates and anisotropic cell behaviour. However, consistent with earlier work[11], we found no evidence for anisotropic distribution of activated Src42A along apical tracheal cell boundaries. Although we cannot exclude subtle local differences or dynamic anisotropy of Src activity, our results suggest that activated Src42A is uniformly distributed at the apical cortex (Supplementary Fig. S2d). Although the relevant Src substrates may be distributed in a planar-polarized fashion in tracheal cells, proteins that exhibit planar-polarized localization in tracheal cells have not been described. We examined the effects of *Src42A* mutations on the localization of potential Src substrates, including signalling, cytoskeletal and junctional proteins. Src activity can induce Jun N-terminal kinase (JNK) phosphorylation[14], which may induce cell shape changes. However, a JNK signalling reporter, *puckered*–lacZ (*puc*–lacZ; ref. 21) was expressed only in a few tracheal cells, and tracheal expression of dominant-negative *bsk* or of the negative JNK regulator *puckered* did not affect dorsal-trunk elongation (data not shown), suggesting that JNK signalling is not involved in Src-dependent tracheal elongation. Furthermore, the apical transmembrane protein Uninflatable (Fig. 1g), subapical proteins (Bazooka–GFP (green fluorescent protein), Crumbs; Supplementary Fig. S4 and data not shown), adherens-junction components (E-Cadherin (E-Cad)–GFP, Armadillo, α-Catenin (α-Cat)–GFP, p120ctn–GFP, Cno–YFP; Fig. 4b and data not shown), septate-junction components (Coracle, Gliotactin–YFP, Discs large–GFP; Supplementary Fig. S4 and data not shown) and the basal protein Basigin–GFP (data not shown) localized correctly to their respective membrane domains in *Src42A* mutants, suggesting that *Src42A* mutations do not affect apical–basal polarity or septate-junction-based tube-length control[10].

We next analysed the effect of *Src42A* mutations or of dominant-negative *Src42A.KM* on cytoskeletal organization. *Src42A* mutations did not affect the distribution of F-actin in circumferential

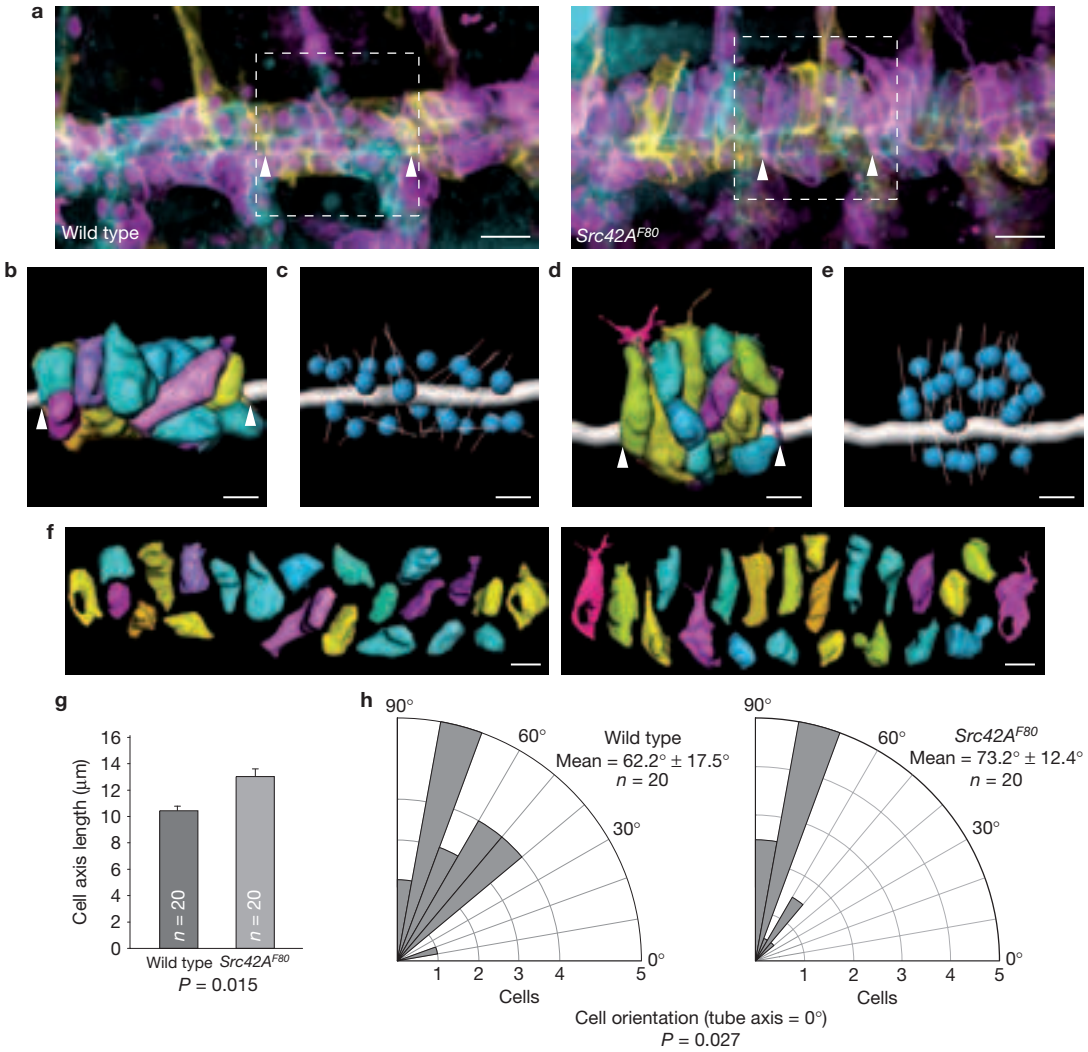

Figure 3 Single-cell analysis reveals altered tracheal cell shapes and epithelial organization in *Src42A* mutants. (**a**) Living late-stage-15 wild-type and *Src42A*^{F80}-mutant embryos expressing upstream activating sequence (UAS)–Brainbow and mCherry–NLS in tracheal cells. Cell membranes are marked by palmitoylated versions of mCherry (magenta), enhanced YFP (eYFP, yellow) or mCerulean (cyan), enabling tracing of the shapes of individual cells. Note that dorsal-trunk cells are cuboidal in the wild type, whereas *Src42A*^{F80} cells are elongated perpendicular to the tube axis. Scale bar, 10 μm. (**b**–**f**) Three-dimensional reconstructions of all dorsal-trunk cells and nuclei in Tr7. Boundaries of Tr7 are marked by white arrowheads. The lumen is shown as a grey tube in **b**–**e**. The longest diagonal within each surface object was used as a measure of cell elongation and is shown as a grey line for each cell in **c** and **e**. Positions of nuclei are shown as blue spheres. (**f**) An 'exploded' view of the cell models. Note that the crowding of cell bodies on the dorsal side of the dorsal trunk in *Src42A* mutants is not due to a change in tracheal cell number (24 ± 1 cells in dorsal trunk Tr8 in *Src42A* mutants versus 21 ± 1 cells in wild-type; $n = 13$; $P = 0.05$). Scale bars in **b**–**f**, 5 μm. (**g**) Length of longest diagonal in wild-type and *Src42A*^{F80}-mutant dorsal-trunk cells. *Src42A*^{F80} mutant cells are strongly elongated perpendicular to the tube axis as compared with wild-type dorsal-trunk cells. Error bars, s.e.m. (**h**) Angle distribution of the longest diagonal of dorsal-trunk cells. The tube axis was set to 0°. Note that dorsal-trunk cells in *Src42A*^{F80} mutants show a strong bias towards a perpendicular orientation relative to the tube axis. The *x* axis indicates the number of cells.

rings (Fig. 4c). Similarly, apical cortical localization of the actin-binding proteins red fluorescent protein (RFP)–Moesin (Supplementary Fig. S4) and Utrophin–GFP (ref. 22), the actin regulators Enabled (Ena/Vasp; ref. 23) and WASp–GFP and the formin Diaphanous (Dia–GFP; Supplementary Fig. S4 and data not shown) was unaffected in *Src42A* mutants or in *Src42A.KM*-expressing embryos. Likewise, microtubule (Supplementary Fig. S4) and spectrin (data not shown) distribution seemed normal in *Src42A*-mutant tracheal cells. In contrast to *Src42A* loss of function, constitutively activated *Src42A* caused disorganization of F-actin rings (Fig. 4c). Src activation also led to ectopic accumulations of Utrophin–GFP and myosin regulatory light chain (MRLC, also known as Sqh)–GFP in spots along basal membranes (Supplementary Fig. S4). These actomyosin foci could account for altered cell shapes on constitutive Src activation. Furthermore, junctional E-Cad–GFP levels were reduced and adherens-junction components (E-Cad–GFP, α-Cat–YFP, Arm–YFP) were mislocalized along basolateral membranes, probably reflecting disassembly and ectopic formation of adherens junctions (Fig. 4d and data not shown).

These findings indicated that Src42A-induced adherens-junction remodelling may promote dorsal-trunk elongation. Src activation leads to phosphorylation and endocytic uptake of E-Cad in mammalian cells[24]. Accordingly, we found that the dynamics, but not steady-state levels, of E-Cad at adherens junctions were altered in *Src42A*^{F80} embryos (Supplementary Fig. S5). Fluorescence recovery after

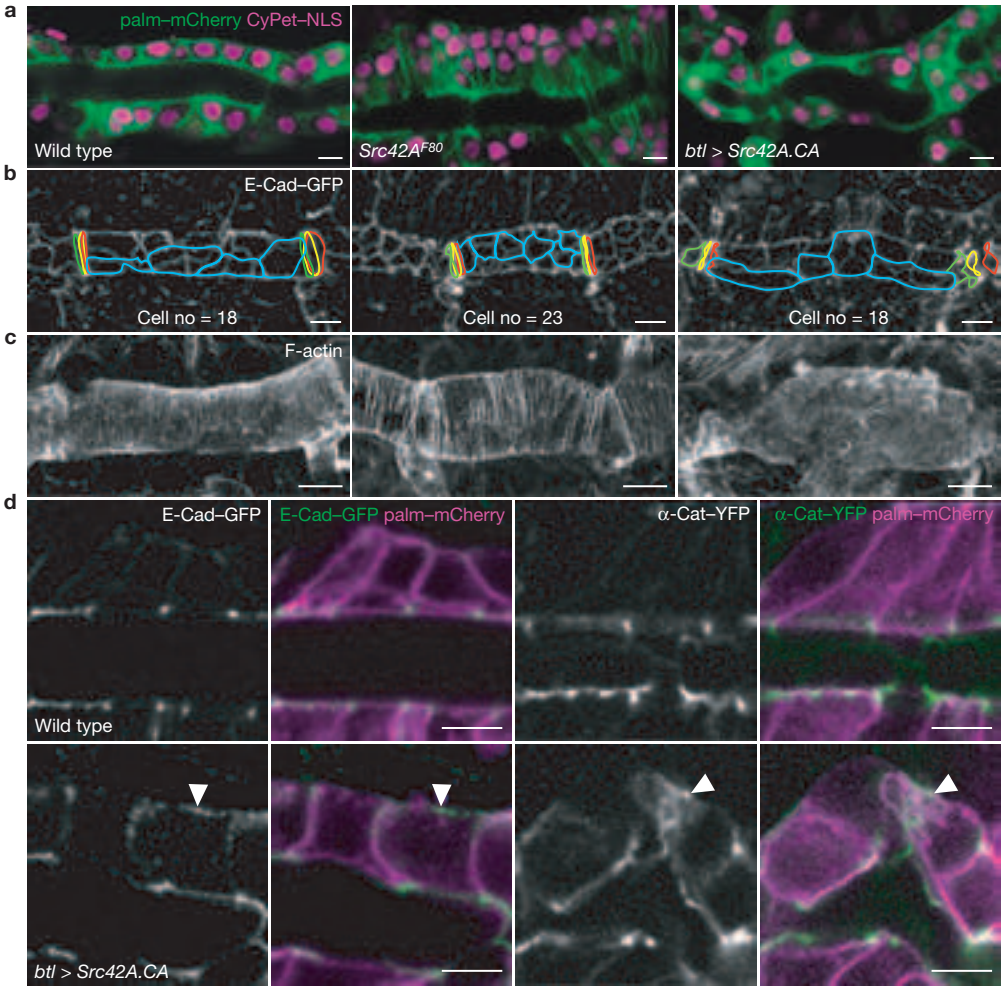

Figure 4 Constitutive activation of Src42A causes excessive tube elongation and abnormal epithelial organization. (**a**–**c**) Comparison of dorsal-trunk cells in Tr8 of living wild-type (left), *Src42A*^{F80}-mutant (middle) and *Src42A.CA*-overexpressing (right) embryos at stage 16. (**a**) Single confocal microscopy sections showing epithelial organization of the dorsal trunk. Tracheal cell membranes are marked by palm–mCherry (green) and nuclei by CyPet–NLS (magenta). Note that the *Src42A*^{F80} mutation leads to a pseudostratified phenotype, whereas activated Src42A leads to overelongated and convoluted tubes with flattened cells. (**b**) Confocal microscopy projections showing E-Cad–GFP-marked outlines of apical cell surfaces. Note the smaller cell surfaces in the *Src42A*^{F80} embryo (middle) and the longitudinally expanded cells in the *Src42A.CA*-overexpressing embryo (right). Also note that Src42A activation leads to mislocalization of E-Cad–GFP to basolateral membranes. The adherens junctions of a frontal row of cells are highlighted in cyan. The junctions of ring-like fusion cells delimiting Tr8 are highlighted in green, yellow and red. Dorsal-trunk cell number in Tr8 is indicated. Note that dorsal-trunk cell number in *Src42A* loss-of-function and gain-of-function situations is not significantly different from that in wild-type controls (*Src42A*^{F80}, 24 ± 1 cells in Tr8 ($n = 11$, $P = 0.66$); *Src42A.CA*, 22 ± 1 cells in Tr8 ($n = 10$, $P = 0.66$); wild type, 21 ± 1 cells in Tr8 ($n = 13$)). (**c**) Phalloidin staining shows apical F-actin organized into regular taenidial rings in wild-type and *Src42A*^{F80} embryos, whereas expression of activated Src42A leads to disorganization of apical F-actin. (**d**) Constitutive activation of Src42A causes mislocalization of adherens junction components. Single confocal microscopy sections of the dorsal trunk in living embryos are shown. Note that E-Cad–GFP and α-Cat–YFP are limited to apical adherens junctions in the wild type (upper panel), but accumulate ectopically in spots along the basolateral membrane (arrowheads) in embryos expressing activated Src42A (lower panel). Merge panels show E-Cad–GFP or α-Cat–YFP in green and a cell-membrane marker (palm–mCherry) in magenta. Scale bars, 5 μm.

photobleaching experiments revealed twofold slower recovery of GFP-tagged endogenous E-Cad (ref. 25) in lateral epidermal cells of *Src42A*^{F80} embryos when compared with controls, suggesting that *Src42A* mutations affect E-Cad recycling at adherens junctions. This is consistent with earlier reports showing reduced dynamics of overexpressed α-Cat–GFP and E-Cad–GFP in *Src42A* mutants[11] and with genetic interactions between *Src42A* and *E-Cad* (also known as *shg*) (ref. 13). These results indicate that *Src42A*-dependent adherens-junction remodelling is limiting for the cell shape changes that mediate dorsal-trunk elongation.

Finally, we asked whether *Src42A*-dependent tube elongation is controlled independently or in concert with other processes that regulate tracheal dimensions. Tube elongation is limited by the apical extracellular matrix proteins Serp and Verm, which are thought to modulate mechanical properties of luminal chitin fibres[8,10]. *serp verm* double mutants show excessively elongated tracheae with long apical cell profiles (Fig. 5a,b). Removing *Src42A* function in *serp verm* mutants results in a phenotype resembling that of *Src42A* mutants, indicating that *Src42A* acts downstream of the tube-length-restricting function of the apical extracellular matrix (Fig. 5c,d). Diametric tube expansion requires luminal secretion[5,6,26]. Mutations in the Sec24 homologue *sten* (also known as *gho*) affect secretion and lead to narrow tracheal lumina with small apical cell surfaces[5] (Fig. 5e,f,k). However, *sten* embryos showed only slightly reduced dorsal-trunk length (Fig. 5k).

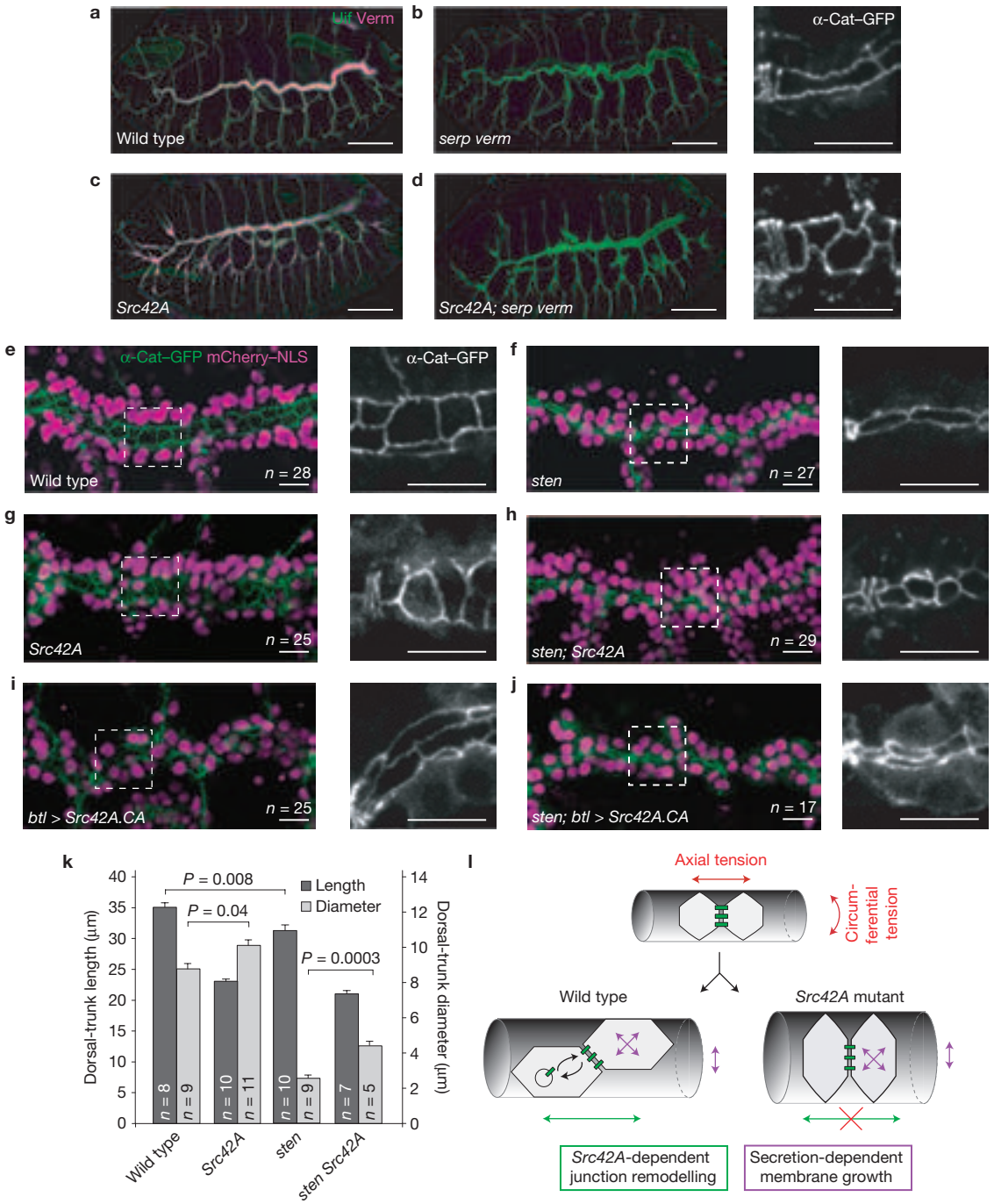

Figure 5 *Src42A* functions downstream of the luminal matrix and independently of exocytosis. (**a**–**d**) Stage-16 wild-type (**a**), $serp^{RB}$ $verm^{KG}$-mutant (**b**), $Src42A^{F80}$-mutant (**c**) and $Src42A^{F80}$; $serp^{RB}$ $verm^{KG}$ triple-mutant (**d**) embryos stained for Uif (green) and Verm (magenta). Right-hand panels show α-Cat–GFP-marked apical cell outlines of living $serp^{RB}$ $verm^{KG}$ (**b**) and $Src42A^{F80}$; $serp^{RB}$ $verm^{KG}$ (**d**) mutants. Note that *Src42A*; *serp verm* mutants show a phenotype resembling that of *Src42A* mutants, indicating that *Src42A* is required downstream of the luminal matrix components Serp and Verm. Scale bars in **a**–**d**, 50 μm; close-ups in **b** and **d**, 10 μm. (**e**–**j**) Living stage-16 wild-type (**e**), $sten^{G200}$ (**f**) and $Src42A^{F80}$ (**g**) single-mutant, $sten^{G200}$ $Src42A^{F80}$ double-mutant (**h**) and wild-type (**i**) or $sten^{G200}$-mutant (**j**) embryos expressing *Src42A.CA* in tracheal cells. Apical cell outlines are visualized using α-Cat–GFP (green) and nuclei using mCherry–NLS (magenta). Numbers of dorsal-trunk cell nuclei (*n*) in Tr8 are indicated. Right-hand panels are single confocal microscopy sections of the boxed regions in Tr7, showing apical cell outlines marked by α-Cat–GFP. Note that *sten* mutants (**f**) show narrow dorsal-trunk lumen, but only slightly reduced tube length when compared with the wild type (**e**). *sten*-mutant dorsal-trunk cells compensate for their smaller surface by stretching axially. This effect requires *Src42A* function (**h**). Conversely, activated Src42A is sufficient to cause dorsal trunk overelongation in *sten* mutants (**j**). Scale bars, 10 μm. (**k**) Graph showing quantification of tube length (left *y* axis) and tube diameter (right *y* axis) in Tr8. Error bars, s.e.m. (**l**) Model for the role of Src42A in tracheal tube elongation. Secretion mediates apical cell surface growth independently of *Src42A* function. *Src42A*-dependent remodelling of adherens junctions (green bars) is required for cell shape changes and cell rearrangements in the axial dimension. Circumferential tension on the cylindrical surface is presumed to be greater than axial tension. Axial cell shape changes and cell rearrangements, which operate orthogonally to the presumed tissue tension, strictly depend on *Src42A* function, whereas circumferential tension may allow for diametric tube expansion in the absence of *Src42A* function.

Interestingly, *sten* embryos showed axially stretched apical cell profiles (Fig. 5f), indicating that the reduced apical membrane growth in *sten* mutants may be partially compensated for by cell shape changes that restore nearly normal tube length, but not tube diameter. Removing *Src42A* function in *sten* embryos abolished compensatory cell elongation and led to short dorsal trunks (Fig. 5h,k). Conversely, constitutive Src42A activation caused overelongated dorsal trunks in *sten* mutants (Fig. 5j), indicating that the ability of Src42A to induce cell elongation may not strictly depend on the secretory apparatus. These results demonstrate that diametric and axial tracheal tube expansion are regulated by distinct cellular processes. Tube elongation depends on *Src42A*-induced polarized cell shape changes, whereas diametric expansion is driven by *sten*-dependent exocytosis.

Our findings establish a critical role of Src in epithelial tube morphogenesis. *Src42A* is necessary and sufficient for cell shape changes that specifically mediate tracheal tube elongation, whereas diametric tube expansion is independent of *Src42A* function. Consistent with previous work[11,24,27], we find that *Src42A* regulates E-Cad recycling at adherens junctions. On the basis of these data we propose that Src42A-induced adherens-junction remodelling is limiting for polarized cell shape changes that mediate axial, but not diametric, dorsal-trunk expansion (Fig. 5l). In this model, secretion drives apical membrane growth independently of *Src42A* function, which is required to direct apical membrane growth in the axial dimension of the tube. However, the signals activating Src42A in tracheal cells and the Src42A substrates mediating polarized cell behaviours remain elusive. We found no evidence for planar-polarized Src activity in tracheal cells or for a role of *Src42A* in PCP signalling, indicating that potential PCP cues that might direct axial expansion may be downstream or parallel to Src42A activity. In principle, even subtle asymmetries in the distribution of adherens-junction components may result in large-scale tissue transformations[22]. Alternatively, polarized cell behaviour may result from the inherent anisotropy imposed by cylindrical geometry of tubular epithelia. On the basis of Laplace's law, circumferential tension on a pressurized cylinder's surface is larger than longitudinal tension. Anisotropic tissue tension might orient cell behaviour in tubular epithelia. Normal epithelial cells cultured on cylindrical substrates orient circumferentially, whereas Ras-transformed cells orient axially, accompanied by re-orientation of actin filaments[28], indicating that cells may be able to sense and respond to tissue geometry. We propose that Src42A is involved in sensing cylindrical tissue geometry, possibly as a mechanical force sensor, or by translating this information into polarized cell behaviour[29,30]. The specific effect of *Src42A* mutations on axial, but not circumferential, cell shape changes may reflect different requirements for Src42A in remodelling axial and circumferential adherens junctions, respectively. A possible explanation for *Src42A* affecting elongation of the dorsal trunk and transverse connective, but not of dorsal branches, whose elongation relies on adherens-junction remodelling[31,32], is that dorsal-branch cell intercalation relies on pulling forces generated by migrating tip cells[33], which may override the *Src42A* requirement. Conversely, the absence of tip-cell-mediated pulling forces in the dorsal trunk and transverse connective may imply an increased requirement for Src42A-mediated junction remodelling in these branches. Our work provides a genetically tractable paradigm to analyse Src function in regulating polarized cell behaviours that control epithelial tube dimensions during normal organogenesis or under pathological conditions, such as polycystic kidney disease, in which Src has been implicated[34]. □

METHODS

Methods and any associated references are available in the online version of the paper at www.nature.com/naturecellbiology

Note: Supplementary Information is available on the Nature Cell Biology website

ACKNOWLEDGEMENTS

We are indebted to K. Armbruster and S. Limmer, who isolated the *Src42A* mutants, and to T. Aegerter-Wilmsen for help with MATLAB analyses. We thank R. Güttinger for help with cell tracking, T. Aegerter-Wilmsen, C. Aegerter, M. Gonzalez-Gaitan, J. Grosshans, R. Metzger and D. Strutt for advice and comments on the manuscript and C. Lehner for support and discussions. We thank M. Affolter, K. Basler, E. Caussinus, J. Grosshans, S. Hayashi, Y. Hong, T. Kojima, T. Lecuit, A. Müller, D. Strutt, R. Ward and T. Xu for providing antibodies and fly stocks and J. Livet for providing Brainbow plasmids. We apologize to colleagues whose work could not be cited owing to space limitations. This work was supported by the German Research Foundation (DFG LU-1398/1-1), the Swiss National Science Foundation (SNF 3100A0_120713), the RPH-Promotor Stiftung, the Julius Klaus-Stiftung Zürich, the University of Zürich and the Kanton Zürich. D.F. was supported by a Müller fellowship of the Zürich Ph.D. programme in Molecular Life Sciences and by the Forschungskredit of the University of Zürich.

AUTHOR CONTRIBUTIONS

D.F. and S.L. designed the experiments, D.F. carried out the experiments, D.F. and S.L. analysed the data. D.F. and S.L. wrote the paper.

COMPETING FINANCIAL INTERESTS

The authors declare no competing financial interests.

Published online at www.nature.com/naturecellbiology
Reprints and permissions information is available online at www.nature.com/reprints

1. Datta, A., Bryant, D. M. & Mostov, K. E. Molecular regulation of lumen morphogenesis. *Curr. Biol.* **21,** R126–R136 (2011).
2. Lubarsky, B. & Krasnow, M. A. Tube morphogenesis: making and shaping biological tubes. *Cell* **112,** 19–28 (2003).
3. Ghabrial, A., Luschnig, S., Metzstein, M. M. & Krasnow, M. A. Branching morphogenesis of the *Drosophila* tracheal system. *Annu. Rev. Cell Dev. Biol.* **19,** 623–647 (2003).
4. Beitel, G. & Krasnow, M. Genetic control of epithelial tube size in the *Drosophila* tracheal system. *Development* **127,** 3271–3282 (2000).
5. Förster, D., Armbruster, K. & Luschnig, S. Sec24-dependent secretion drives cell-autonomous expansion of tracheal tubes in *Drosophila*. *Curr. Biol.* **20,** 62–68 (2010).
6. Tsarouhas, V. *et al*. Sequential pulses of apical epithelial secretion and endocytosis drive airway maturation in *Drosophila*. *Dev. Cell* **13,** 214–225 (2007).
7. Devine, W. P. *et al*. Requirement for chitin biosynthesis in epithelial tube morphogenesis. *Proc. Natl Acad. Sci. USA* **102,** 17014–17019 (2005).
8. Luschnig, S., Bätz, T., Armbruster, K. & Krasnow, M. *serpentine* and *vermiform* encode matrix proteins with chitin binding and deacetylation domains that limit tracheal tube length in *Drosophila*. *Curr. Biol.* **16,** 186–194 (2006).
9. Tonning, A. *et al*. A transient luminal chitinous matrix is required to model epithelial tube diameter in the *Drosophila* trachea. *Dev. Cell* **9,** 423–430 (2005).
10. Wang, S. *et al*. Septate-junction-dependent luminal deposition of chitin deacetylases restricts tube elongation in the *Drosophila* trachea. *Curr. Biol.* **16,** 180–185 (2006).
11. Shindo, M. *et al*. Dual function of Src in the maintenance of adherens junctions during tracheal epithelial morphogenesis. *Development* **135,** 1355–1364 (2008).
12. Takahashi, F., Endo, S., Kojima, T. & Saigo, K. Regulation of cell–cell contacts in developing *Drosophila* eyes by Dsrc41, a new, close relative of vertebrate c-src. *Genes Dev.* **10,** 1645–1656 (1996).
13. Takahashi, M., Takahashi, F., Ui-Tei, K., Kojima, T. & Saigo, K. Requirements of genetic interactions between *Src42A*, *armadillo* and *shotgun*, a gene encoding E-cadherin, for normal development in *Drosophila*. *Development* **132,** 2547–2559 (2005).
14. Tateno, M., Nishida, Y. & Adachi-Yamada, T. Regulation of JNK by Src during *Drosophila* development. *Science* **287,** 324–327 (2000).
15. Matusek, T. *et al*. The *Drosophila* formin DAAM regulates the tracheal cuticle pattern through organizing the actin cytoskeleton. *Development* **133,** 957–966 (2006).
16. Chung, S. *et al*. Serrano (sano) functions with the planar cell polarity genes to control tracheal tube length. *PLoS Genet.* **5,** e1000746 (2009).

17. Usui, T. *et al.* Flamingo, a seven-pass transmembrane cadherin, regulates planar cell polarity under the control of Frizzled. *Cell* **98,** 585–595 (1999).
18. Strutt, D., Johnson, R., Cooper, K. & Bray, S. Asymmetric localization of frizzled and the determination of notch-dependent cell fate in the *Drosophila* eye. *Curr. Biol.* **12,** 813–824 (2002).
19. Strutt, D. I. Asymmetric localization of frizzled and the establishment of cell polarity in the *Drosophila* wing. *Mol. Cell* **7,** 367–375 (2001).
20. Livet, J. *et al.* Transgenic strategies for combinatorial expression of fluorescent proteins in the nervous system. *Nature* **450,** 56–62 (2007).
21. Martin-Blanco, E. *et al. puckered* encodes a phosphatase that mediates a feedback loop regulating JNK activity during dorsal closure in *Drosophila*. *Genes Dev.* **12,** 557–570 (1998).
22. Rauzi, M., Lenne, P. F. & Lecuit, T. Planar polarized actomyosin contractile flows control epithelial junction remodelling. *Nature* **468,** 1110–1114 (2010).
23. Choi, W. *et al.* The single *Drosophila* ZO-1 protein Polychaetoid regulates embryonic morphogenesis in coordination with Canoe/Afadin and Enabled. *Mol. Biol. Cell* **22,** 2010–2030 (2011).
24. Fujita, Y. *et al.* Hakai, a c-Cbl-like protein, ubiquitinates and induces endocytosis of the E-cadherin complex. *Nat. Cell Biol.* **4,** 222–231 (2002).
25. Huang, J., Zhou, W., Dong, W., Watson, A. M. & Hong, Y. Directed, efficient, and versatile modifications of the *Drosophila* genome by genomic engineering. *Proc. Natl Acad. Sci. USA* **106,** 8284–8289 (2009).
26. Grieder, N. C. *et al.* γCOP is required for apical protein secretion and epithelial morphogenesis in *Drosophila melanogaster*. *PLoS One* **3,** e3241 (2008).
27. Gumbiner, B. M. Regulation of cadherin-mediated adhesion in morphogenesis. *Nat. Rev. Mol. Cell Biol.* **6,** 622–634 (2005).
28. Levina, E. M., Domnina, L. V., Rovensky, Y. A. & Vasiliev, J. M. Cylindrical substratum induces different patterns of actin microfilament bundles in nontransformed and in ras-transformed epitheliocytes. *Exp. Cell Res.* **229,** 159–165 (1996).
29. Han, B. *et al.* Conversion of mechanical force into biochemical signaling. *J. Biol. Chem* **279,** 54793–54801 (2004).
30. Wang, Y. *et al.* Visualizing the mechanical activation of Src. *Nature* **434,** 1040–1045 (2005).
31. Ribeiro, C., Neumann, M. & Affolter, M. Genetic control of cell intercalation during tracheal morphogenesis in *Drosophila*. *Curr. Biol.* **14,** 2197–2207 (2004).
32. Shaye, D. D., Casanova, J. & Llimargas, M. Modulation of intracellular trafficking regulates cell intercalation in the *Drosophila* trachea. *Nat. Cell Biol.* **10,** 964–970 (2008).
33. Caussinus, E., Colombelli, J. & Affolter, M. Tip-cell migration controls stalk-cell intercalation during *Drosophila* tracheal tube elongation. *Curr. Biol.* **18,** 1727–1734 (2008).
34. Sweeney, W. E., von Vigier, R. O., Frost, P. & Avner, E. D. Src inhibition ameliorates polycystic kidney disease. *J. Am. Soc. Nephrol.* **19,** 1331–1341 (2008).

DOI: 10.1038/ncb2456

METHODS

***Drosophila* stocks.** The following fly stocks were used: *Abd-B*–Gal4 (199; ref. 5), *en*–Gal4, UAS–α-Cat–GFP (ref. 35), UAS–mCherry–NLS (ref. 33), UAS–CyPet–NLS (gift from E. Caussinus and M. Affolter), UAS–myr–GFP (='UAS–Src–GFP'), UAS–myr–mRFP, Df(2R)nap14, ubi-p120ctn–GFP, *hsp70-Mos1*–Cre (Bloomington stock centre), $Src42A^{26-1}$ (gift from T. Kojima; ref. 13), UAS–*Src42A.CA* (Y511F; ref. 14), UAS–*Src42A.KM* (K295M; ref. 11), UAS–*Src42A*[67], UAS–*Src42A*[30-2], UAS–*Src42A*[16-2] (gift from T. Xu; ref. 36), DE-Cad–GFP, DE-Cad–mTomato (gift from Y. Hong; ref. 25), $sten^{G200}$ (ref. 5), $serp^{RB}$ $verm^{KG}$ (ref. 8), Baz–GFP, Dlg–GFP (ref. 37), Gli–YFP, α-Cat–YFP, Arm–YFP, Cno–YFP (Kyoto stock centre), *btl*-mRFP–Moe (ref. 31), Sqh–GFP, *sqh*–Utrophin–GFP (ref. 22), UASp–GFP–Dia (gift from J. Grosshans), UAS–WASp–GFP (gift from A. Müller) and *Act5c*–Stbm–YFP (also known as Vang-YFP; ref. 18). New insertions of *btl*–Gal4 (ref. 38) on the X and third chromosome were generated by P-transposase-mediated mobilization.

Isolation of *Src42A* mutations. *Src42A* mutants were isolated in an ethylmethane sulphonate mutagenesis screen as previously described[5]. The F80 and K147 mutations were mapped to the cytological interval 42A1–42B1 by non-complementation of Df(2R)nap9 and Df(2R)nap14 (FlyBase). The *Src42A* coding sequence, including exon–intron boundaries, was amplified by PCR from homozygous mutant embryos and from the parental strain. The point mutations in $Src42A^{F80}$ and $Src42A^{K147}$ were identified by sequencing PCR products with oligonucleotides Src42A-72F (5′-TGCATGCATTTTAATAATTTCCT-3′), Src42A-73R (5′-ATGCGCGATTAAATCAAAGC-3′), Src42A-74F (5′-GCTGTGCAGTACTACGCCTAAA-3′) and Src42A-81R (5′-ACGATGTTTCCATCGCCTAC-3′).

UAS–Brainbow transgene and Cre-induced recombination. The Brainbow-1.1-M cassette[20] (carrying Kusabira Orange, palm–mCherry, palm–eYFP, and palm–mCerulean open reading frames) was inserted as an EcoRI/XhoI fragment into the pUAST vector. Transgenic flies were generated by standard P-element transformation. To induce Cre/lox recombination in tracheal cells, UAS–Brainbow males were crossed to females carrying a constitutively expressed *hsp70-Mos1*–Cre transgene and *btl*–Gal4. Crosses were maintained at 22°. Cre recombinase acts on pairs of compatible lox sites, recombination of which results in a stochastic pattern of cells expressing palmitoylated mCherry, eYFP or mCerulean at approximately equal frequencies. *btl*-Gal4 UAS–palmYFP, *btl*-Gal4 UAS–palmCherry and *btl*–Gal4 UAS–palmCerulean lines were generated by Cre-induced recombination of the UAS–Brainbow construct in the female germline after recombining a second-chromosomal insertion of UAS–Brainbow with *btl*–Gal4.

Immunohistochemistry and antibodies. The following primary antibodies were used: rabbit anti-Verm (1:300; ref. 8), mouse anti-GFP 7.1/13.1 (1:500; Roche 11814460001), guinea pig anti-Uif (1:1,000; ref. 39), mouse anti-α-tubulin DM1A (1:8,000; Sigma T6199), mouse anti-α-spectrin 3A9 (1:50; DSHB), rat anti-E-Cad DCAD2 (1:100; DSHB), rabbit anti-Src42A (1:200; ref. 13), rabbit anti-pSrc42A (1:500, gift from S. Hayashi), mouse anti-Ena 5G2 (1:50; DSHB), mouse anti-Fmi no 74 (1:10; DSHB). Rhodamine- or fluorescein isothiocyanate-conjugated chitin-binding probe (1:100; New England Biolabs) was used to detect chitin. Tetramethylrhodamine isothiocyanate-conjugated phalloidin (1:40; Sigma) was used to detect F-actin. Secondary antibodies were conjugated with Alexa 488, Alexa 568 (Molecular Probes) or Cy5 (Jackson ImmunoResearch). Embryos were fixed in 4% formaldehyde in PBS–heptane for 20 min and devitellinized by shaking in methanol–heptane or (for anti-E-Cad and phalloidin stainings) in ethanol–heptane. Pupal wings (30 h after puparium formation) were stained as previously described[19].

Light microscopy. For live imaging experiments embryos were dechorionated, lined up on a glue-coated coverslip and covered with Voltalef 10S oil. Imaging was carried out using an Olympus FV1000 confocal microscope equipped with a 488 nm argon and 405 nm, 559 nm and 635 nm diode lasers and ×40/1.3 numerical aperture (NA) and ×60/1.35 NA objectives, or on a Leica SP5 confocal microscope equipped with a 488 nm argon laser and a ×63/1.4 NA objective. Unless stated otherwise, maximum-intensity projections of Z-stacks of tracheal dorsal-trunk metameres 6–8 are shown. Images were processed using Huygens Deconvolution (SVI), ImageJ (v1.42; NIH), Imaris (v7.3.0; Bitplane) and Adobe Photoshop. For time-lapse imaging of tracheal development, embryos were collected 9 h after egg lay and filmed with 3 min intervals (×40/1.3 NA objective; Supplementary Movie S1), or 5 min intervals (×60/1.35 NA objective; Supplementary Fig. S3). Time-lapse imaging of apical cell surface changes (Supplementary Movie S2 and Fig. 2f) was carried out with 90 s intervals beginning at 11 h after egg lay (×60/1.35 NA objective). Time-lapse movies were processed using the StackReg plugin in ImageJ to correct for drift in the *xy* plane.

Fluorescence recovery after photobleaching experiments. Wild-type and $Src42A^{F80}$-mutant embryos, in which the only source of E-Cad is a GFP-tagged protein produced by an E-Cad–GFP knock-in construct[25], were analysed. Embryos were imaged at 25 °C using an argon laser (488 nm) and a ×60/1.35 NA oil lens on an Olympus FV1000 confocal microscope equipped with two laser scanners. Pre- and post-bleach images were 90 × 110 pixels (1 pixel = 110 nm), each line averaged three times, with a 474 ms frame rate and no delay between consecutive images. After acquisition of 50 pre-bleach scans, an area of 10 × 10 pixels (=1.21 μm^2) in the epidermis was bleached using a 405 nm diode laser at 50% power. Fluorescence recovery was monitored over at least 3.3 min. To measure fluorescence intensities, fluorescence recovery after photobleaching data without focus drift was selected. The StackReg plugin in ImageJ was used to correct for movement of the embryo in the *xy* plane. As a control region of interest the entire junction between the two vertices bearing the bleach region of interest was analysed. Fluorescence intensities were measured using the ROI Manager of ImageJ. Igor Pro software (Wavemetrics) was used for normalization (back-multiplication method), curve fitting (single-exponential fit), and calculation of recovery half-times.

Quantification and statistics. All measurements were carried out on confocal Z-stacks of living embryos in three dimensions using Imaris. Unless mentioned otherwise, embryos were at stage 16. Embryo length was measured in E-Cad–GFP-expressing embryos. Dorsal-trunk luminal length was measured between fusion joints of dorsal-trunk metameres Tr7/8 and Tr8/9. Dorsal-trunk lumen diameter was measured at three defined positions in Tr8, and values were averaged (Tr7/8 dorsal-trunk fusion joint +5 μm, middle of Tr8 dorsal trunk, Tr8/9 dorsal-trunk fusion joint −5 μm). Dorsal-branch length was measured as previously described[33]. TC length was measured from the adherens junction connecting the first transverse-connective cell to the dorsal trunk, to the lateral trunk branching point. Dorsal-trunk cell number was counted according to apical cell surfaces labelled with E-Cad–GFP or α-Cat–GFP. To quantify apical cell surfaces, E-Cad–GFP or α-Cat–GFP outlines were manually traced in Imaris, and their *xyz* Cartesian coordinates were exported. Using a custom MATLAB (v. R2010a, MathWorks) code the coordinates were rotated around the *z* axis such that the *x* axis was parallel to the tube axis. The curvature of the luminal cell surface was taken into account by unfolding the cell surfaces, assuming a perfectly round lumen with a radius determined from the image data. The resulting projection in the *xy* plane was used for the calculations. To validate measurements of single-cell apical surface areas, the total luminal surface area of Tr8 (assuming perfect cylindrical geometry of the tube) was calculated and divided by the number of cells. The average values for cell surface areas obtained using these two independent approaches differed by ±1.5%, thus validating the consistency of the two methods. The algorithms to calculate elongation and orientation of the projected apical outlines were adopted from ref. 40. OpenRose software (v0.01, SourceForge) was used to plot angle distributions.

To measure junction curvature, α-Cat–GFP-marked junctions were classified according to the angle (relative to the tube axis) of a straight line between two vertices at $t = 0$ (axial junctions, 0° ± 30°; circumferential junctions, 90° ± 30°). The line tool in ImageJ was used to measure distances between vertices. α-Cat–GFP-marked junctions between two vertices were automatically traced and their length was measured using the Simple Neurite Tracer plugin in ImageJ. The ratio of junction length and vertex distance was used as a measure for junction curvature (a perfectly straight junction has a ratio of 1).

Surface renderings of single dorsal-trunk cells were created semi-automatically using the Contour Drawing Mode in Imaris. The longest diagonal within a cell surface object was used as a measure for cell elongation. Two independent methods were used to quantify cell orientation. First, the orientation of the longest diagonal inside each cell surface object was determined empirically. Second, for each cell the best-fitting ellipsoid was determined by Imaris, defined by the three principal axes *a*, *b* and *c*. The longest ellipsoid axis (*c*) was used as a measure for orientation of the cell relative to the tube axis. The two methods yielded comparable results for both cell axis length and orientation. Tracheal fusion cells were excluded from all analyses. All data are mean values ± s.e.m. with *P* values calculated by Student's two-tailed, unpaired *t*-test.

35. Oda, H. & Tsukita, S. Dynamic features of adherens junctions during *Drosophila* embryonic epithelial morphogenesis revealed by a Dα-catenin–GFP fusion protein. *Dev. Genes Evol.* **209,** 218–225 (1999).
36. Pedraza, L. G., Stewart, R. A., Li, D-M. & Xu, T. *Drosophila* Src-family kinases function with Csk to regulate cell proliferation and apoptosis. *Oncogene* **23,** 4754–4762 (2004).
37. Buszczak, M. *et al.* The Carnegie protein trap library: a versatile tool for *Drosophila* developmental studies. *Genetics* **175,** 1505–1531 (2007).
38. Shiga, Y., Tanaka-Matakatsu, M. & Hayashi, S. A nuclear GFP/β-galactosidase fusion protein as a marker for morphogenesis in living *Drosophila*. *Dev. Growth Diffn.* **38,** 99–106 (1996).
39. Zhang, L. & Ward, R. E. t. Uninflatable encodes a novel ectodermal apical surface protein required for tracheal inflation in *Drosophila*. *Dev. Biol.* **336,** 201–212 (2009).
40. Aubouy, M., Jiang, Y., Glazier, J. A. & Graner, F. A texture tensor to quantify deformations. *Granular Matter* **5,** 67–70 (2003).

nature cell biology

DOI: 10.1038/ncb2456

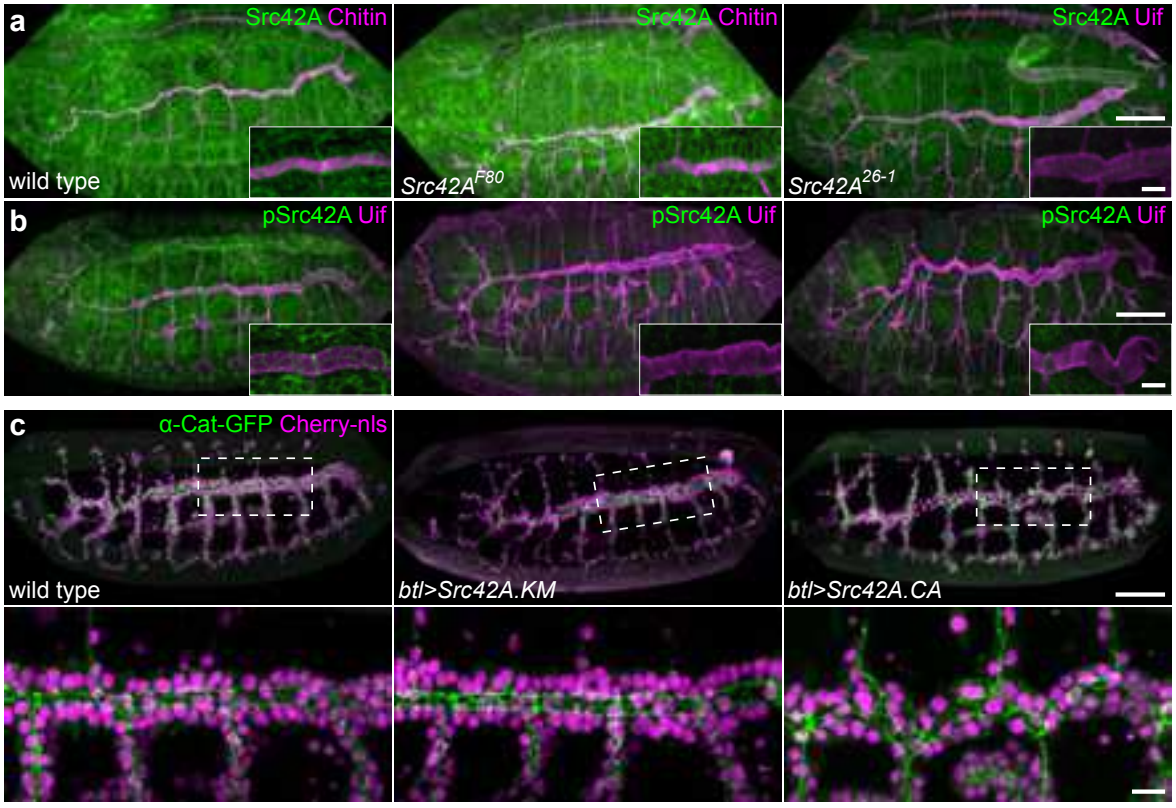

Figure S1 *Src42A*^{F80} is a loss of function mutation that renders Src42A protein non-activatable. (a, b) Stage 16 wild-type embryo (left), *Src42A*^{F80} mutant (middle), and *Src42A*$^{26\text{-}1}$ deletion mutant (right) stained for Src42A protein (green in a) or for activated Src42A protein phosphorylated on Tyr400 (pSrc; green in b) and either Uif or Chitin (magenta) to visualize the tracheal lumen. Insets show close-ups of the tracheal DT. Note that wild-type Src42A protein localizes to cell membranes, whereas activated Src42A is limited to the apical marginal zone (see inset in b). In *Src42A*^{F80} mutants Src42A protein is present and membrane-localized, but fails to get activated, while in *Src42A*$^{26\text{-}1}$ deletion mutants Src42A-specific signals are strongly reduced or absent. Green signals in the hindgut of *Src42A*$^{26\text{-}1}$ embryos (a; right panel) are likely to be due to a cross-reaction of the anti-Src42A antiserum. Note that tube elongation defects of *Src42A*^{F80} embryos (middle panels) are slightly stronger than those of the *Src42A*$^{26\text{-}1}$ null allele (right panels). Scale bars: whole embryos, 50 μm; insets, 10 μm. (c) Living stage 15 embryos expressing α-Cat-GFP (green) and mCherry-nls (magenta) in tracheal cells. The lower panels show close-ups of DT metameres Tr6-8 marked by the boxed regions. Tracheal Expression of *Src42A.KM* (middle panel) results in short DT, while *Src42A.CA* expression (right panel) results in overelongated DT compared to the wild type (left panel). *Src42A.CA* overexpressing embryos displayed partially penetrant DT lumen fusion defects (not shown). Tube length was measured in single tracheal metameres of intact DTs. Scale bars: upper panels, 50 μm; lower panels (close-ups), 10 μm.

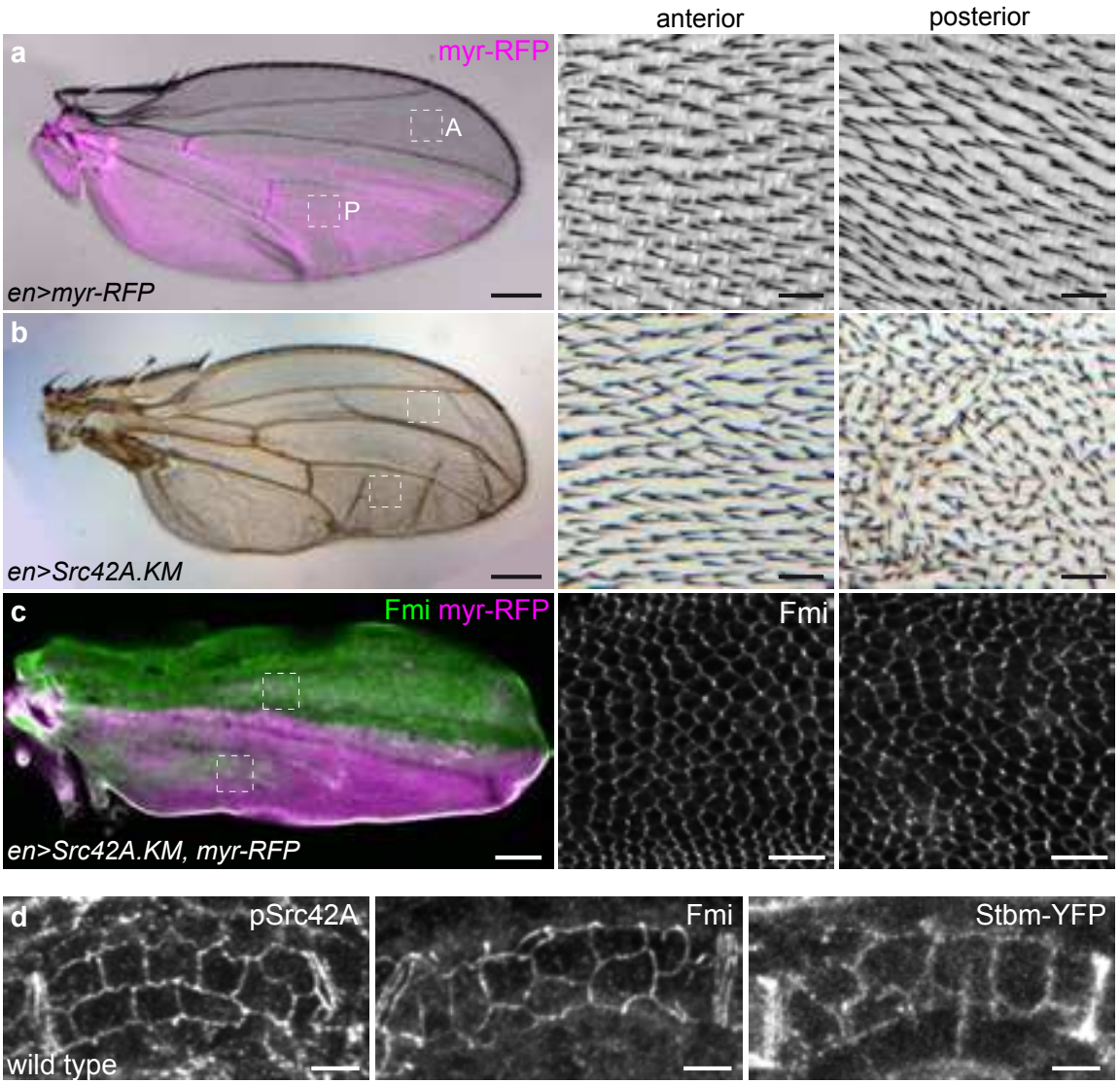

Figure S2 Dominant-negative *Src42A* does not interfere with planar cell polarity signalling. (a-c) Adult (a, b) or pupal (c) wings are shown. All wings express myr-RFP (magenta) driven by *en-Gal4* to mark the posterior compartment (myr-RFP is not shown in b). Close-ups of the areas marked by boxes in the anterior (A) and posterior (P) compartment are shown to the right. *en-Gal4*-driven expression of dominant-negative *Src42A* leads to reduced wing size and disorganized wing hairs in the posterior compartment (b). However, the polarized localization of Fmi at proximal and distal cell junctions in pupal wings is not affected by dominant-negative Src42A expression (c), although the stereotypic hexagonal packing of cells is slightly disturbed. Scale bars for adult wings (a, b), 200 μm; close-ups, 20 μm. Scale bars for pupal wing (c), 50 μm; close-ups, 10 μm. (d) Stage 16 tracheal DT (Tr8) in fixed (left, middle) or living (right) wild-type embryos showing the localization of pSrc (left), Fmi (middle), or Stbm-YFP (right) at apical cell boundaries. Note that pSrc, Fmi, and Stbm-YFP are distributed along DT cell junctions. Planar polarized distribution of pSrc, Fmi, or Stbm-YFP was not observed in the DT. Scale bars, 5 μm.

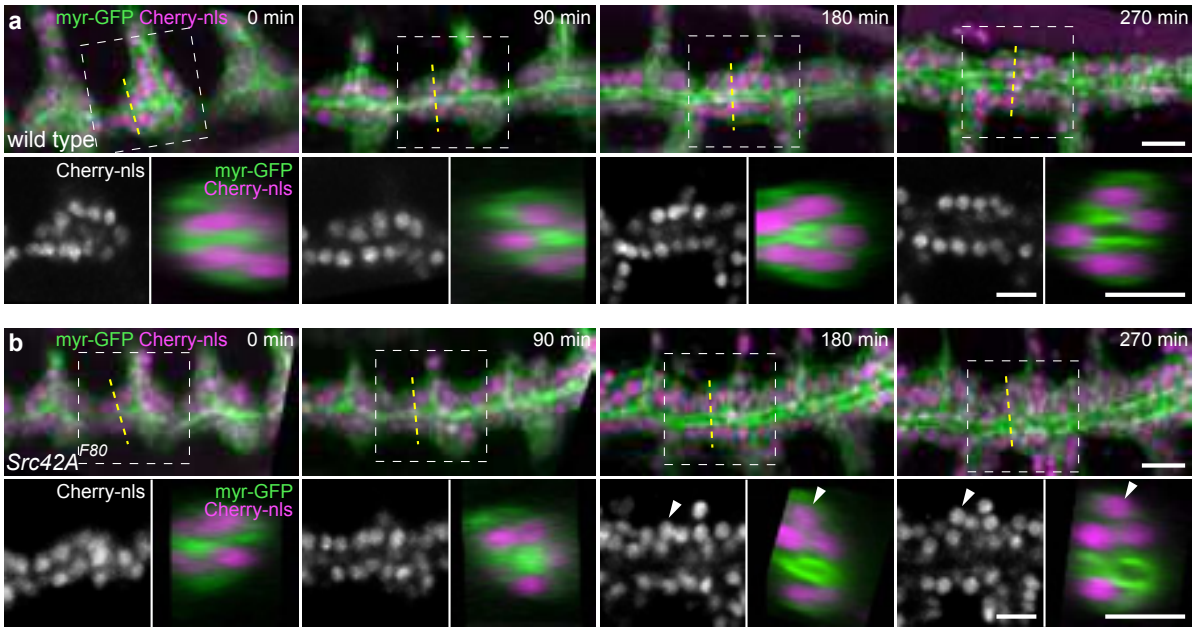

Figure S3 Defects in tube elongation and epithelial organization in *Src42A* mutants arise simultaneously at the onset of tube expansion. (a, b) Stills from time-lapse movies of a wild-type (a) and a *Src42A*^{F80} mutant (b) embryo (see also Supplementary Movie 1). Tracheal cells are marked by myr-GFP (green) and nuclei are marked by mCherry-nls (magenta) expressed under the control of *btl*-Gal4. Upper panels show tracheal metameres Tr6-8. Time in minutes is indicated. For each time point, lower panels to the left show the distribution of nuclei in Tr7 and lower panels to the right show tube cross-sections in Tr7. Position of Tr7 is indicated by boxes and the planes of the cross-sections are indicated by dashed lines in the upper panels. While early tracheal development, including DT tube fusion (0-90 min), is not affected in *Src42A* mutants, defects in tube elongation become apparent at late stage 14 (180 min). DT cells in the *Src42A*^{F80} mutant begin to elongate dorsally and their nuclei are displaced dorsally (180-270 min), thus creating the impression of a multilayered epithelium. Note the stacking of nuclei beginning at 180 min in the *Src42A*^{F80} mutant (arrowheads). Scale bars: upper panels, 10 μm; lower panels, 5 μm.

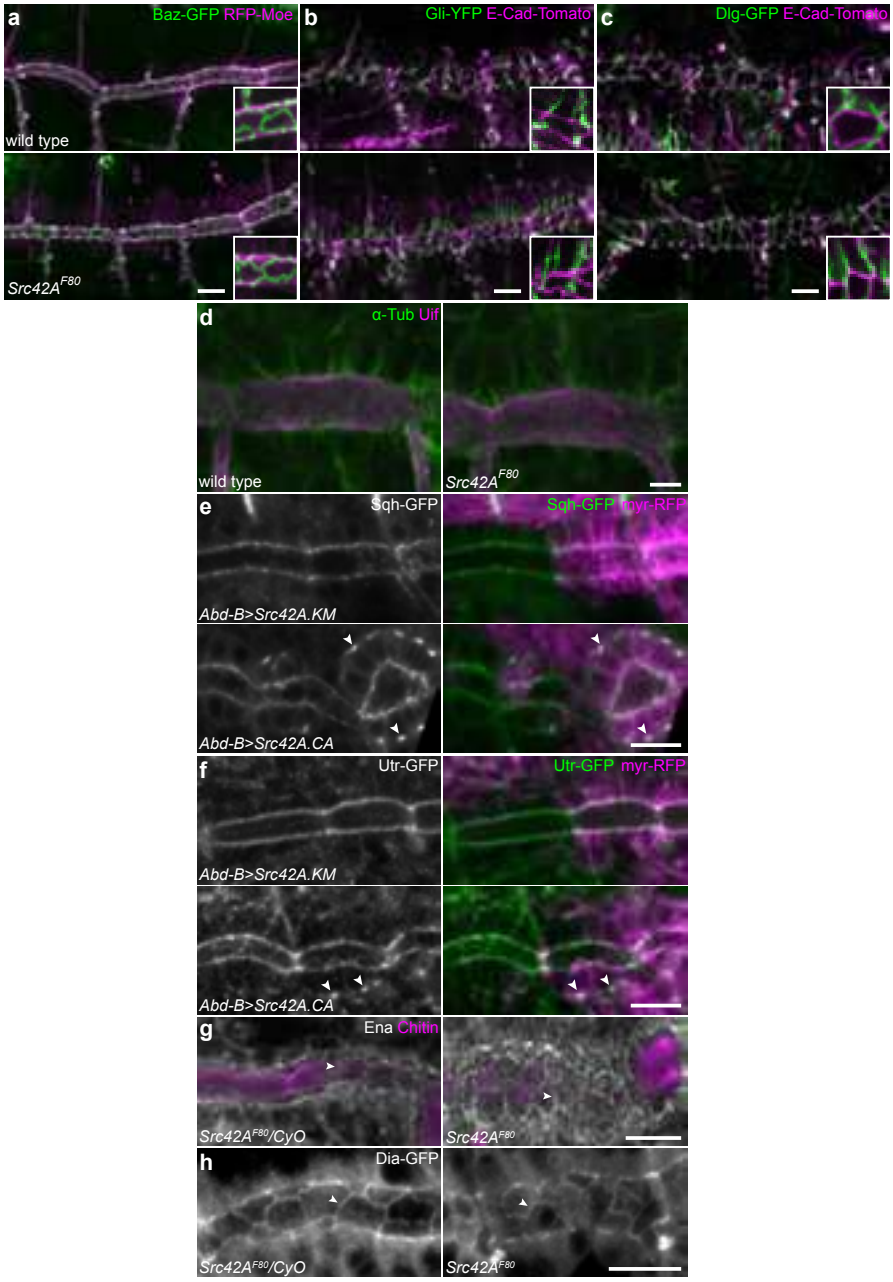

Figure S4 *Src42A* mutations do not affect epithelial polarity and actomyosin localisation, whereas constitutive Src42A activation leads to ectopic actomyosin accumulation. (a-c) Tracheal DT in living stage 16 wild-type (top panels) and *Src42A*^{F80} mutant (bottom panels) embryos. Fluorescent fusion proteins tagged at the endogenous gene loci were used (Baz-GFP, Gli-YFP, E-Cad-Tomato, Dlg-GFP). RFP-Moe expression was driven by the *btl* enhancer. Insets are close-ups of Tr7. Note that the subcellular localization of all proteins tested appeared normal in *Src42A*^{F80} mutants. Scale bars, 10 µm. (d) Tracheal DT in fixed stage 14 wild-type (left) and *Src42A*^{F80} mutant (right) embryos stained for α-Tubulin (green) and Uif (magenta). No discernible effects on the organization of microtubules were observed. Scale bar, 10 µm. (e, f) Living stage 16 embryos expressing dominant-negative (*Src42A.KM*) or constitutive-active (*Src42.CA*) Src42A in posterior tracheal cells driven by *Abd-B*-Gal4, indicated by expression of myr-RFP (magenta). Levels and localization of Sqh-GFP (e, green) and Utr-GFP (f, green), both expressed under the control of the *sqh* promoter, are not affected by *Src42A* loss-of-function, while constitutive Src42A activation leads to punctate accumulations of Sqh-GFP and Utr-GFP at basal cell membranes (arrowheads). Note the short tube phenotype in *Src42A.KM* expressing metameres. Scale bars, 10 µm. (g) Fixed stage 16 *Src42A*^{F80} heterozygous (left panel) or homozygous (right panel) mutant embryos stained for the actin regulator Enabled (Ena, white) and Chitin (magenta). Ena is localized at apical cell boundaries (arrowheads) in wild-type embryos and in *Src42A* mutants. Scale bar, 10 µm. (h) Living stage 16 *Src42A*^{F80} heterozygous (left panel) or homozygous (right panel) mutant embryos expressing Dia-GFP under the control of *btl*-Gal4. Localization of Dia-GFP to apical cell borders (arrowheads) is not affected in *Src42A* mutants. Scale bar, 10 µm.

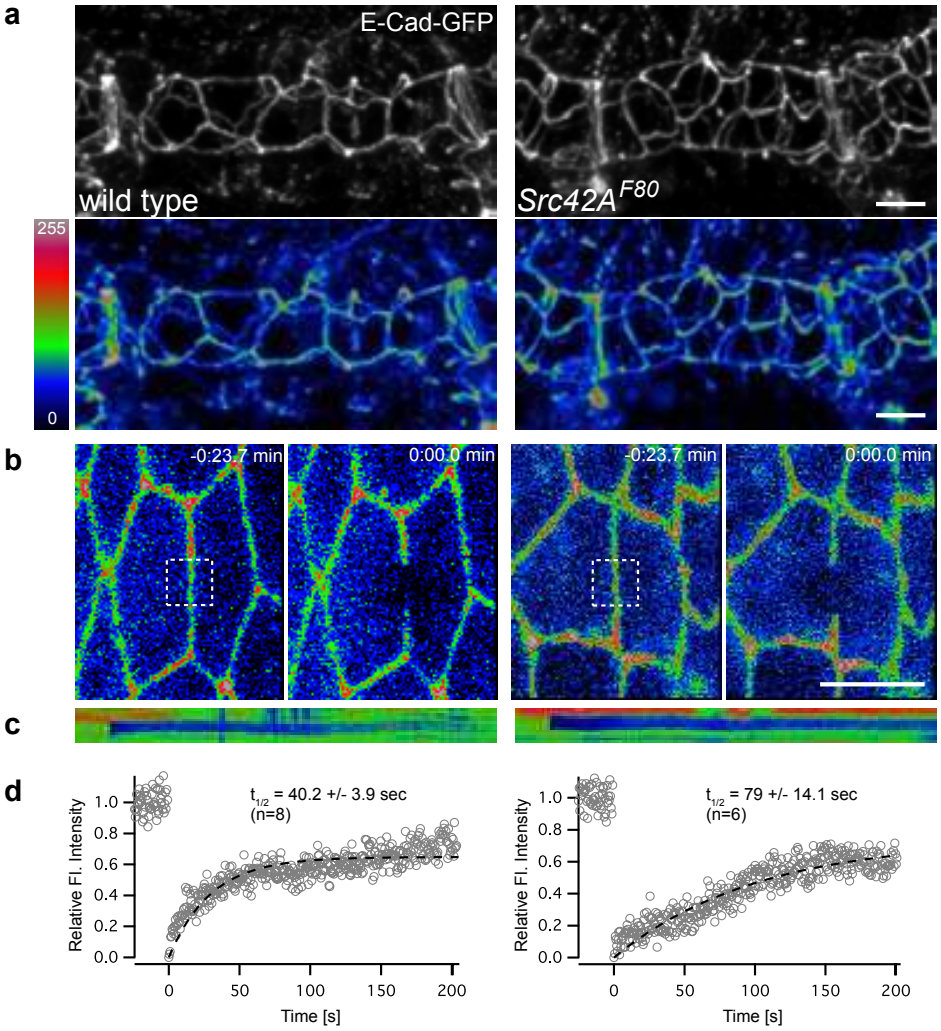

Figure S5 Dynamic turnover, but not steady-state levels, of E-Cadherin at adherens junctions is reduced in *Src42A* mutants. (a) Tracheal DT (Tr8) in stage 16 wild-type and *Src42A*^{F80} mutant embryos, in which the only source of E-Cad is an E-Cad-GFP fusion protein expressed from the endogenous E-Cad locus[25]. Lower panels show E-Cad-GFP signal intensities colour-coded using the heat-map shown on the left. Note that steady-state mean intensities of E-Cad-GFP at AJs are not significantly different between wild-type and *Src42A*^{F80} embryos (p=0.61, n=9). Scale bar, 10 µm. (b) FRAP experiments of E-Cad-GFP in the lateral epidermis of wild-type (left) and *Src42A*^{F80} mutant (right) embryos at stage 14. (b) Images acquired before and just after bleaching are shown. The bleached area is indicated by a white rectangle. Signal intensities are indicated on the heat map shown on the left in (a). Scale bar, 5 µm. (c) Kymographs of the bleached areas indicate that fluorescence recovery in the bleached region is not due to lateral diffusion of E-Cad-GFP. (d) Fluorescence recovery curves (single exponential fit) for the examples shown above. Note that half-maximal recovery times of E-Cad-GFP signals in *Src42A*^{F80} embryos are on average two-fold longer than in the wild type (p=0.04). Values shown for half-maximal recovery times are mean values ± s.e.m.

Supplementary Movies

Movie S1 Time-lapse movie of wild-type (upper frames) and *Src42A*^{F80} mutant (lower frames) embryos expressing myr-GFP (green) and mCherry-nls (magenta) in tracheal cells. Images were acquired every 3 minutes over 6 h (from stage 12 to stage 16). Note that early tracheal development in the *Src42A* mutant proceeds normally until stage 14 (approximately 12 h after egg lay), when tube elongation defects first become apparent in the DT.

Movie S2 Time-lapse imaging of wild-type (upper frames) and *Src42A*^{F80} mutant (lower frames) embryos expressing α-Cat-GFP in tracheal cells. Embryos are at late stage 14 at the beginning of the movies. Images were acquired every 90 seconds over 130 min. While wild-type DT cells expand their apical surfaces both axially and circumferentially and undergo cell rearrangements, apical cell profiles in the *Src42A* mutant expand more slowly and only circumferentially, but not axially. Note that cell boundaries in the wild type remain relatively straight during tube expansion, while they become corrugated in the *Src42A* mutant. See Figure 2f for movie stills.

Movie S3 Living late stage 15 wild-type embryo expressing UAS-Brainbow and UAS-mCherry-nls in tracheal cells. Three-dimensional surface models of DT cells are shown for Tr7. The lumen is visualized as a grey tube. Note that wild-type cells are cuboidal and are distributed around the lumen.

Movie S4 Living late stage 15 *Src42A*^{F80} mutant embryo expressing UAS-Brainbow and UAS-mCherry-nls in tracheal cells. Three-dimensional surface models of DT cells are shown for Tr7. The lumen is visualized as a grey tube. Note that although *Src42A* mutant cells are elongated perpendicular to the tube axis, their apical surfaces are in contact with the lumen.